Journal Pre-proof

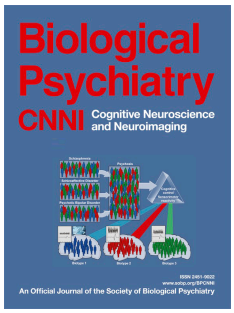

Dysfunctional cortical gradient topography in treatment resistant major depression

Lorenzo Pasquini, Susanna L. Fryer, Stuart J. Eisendrath, Zindel V. Segal, Alex J. Lee, Jesse A. Brown, Manish Saggar, Daniel H. Mathalon

PII: S2451-9022(22)00270-1

DOI: https://doi.org/10.1016/j.bpsc.2022.10.009

Reference: BPSC 1020

To appear in: *Biological Psychiatry: Cognitive Neuroscience and Neuroimaging*

Received Date: 14 June 2022

Revised Date: 13 October 2022

Accepted Date: 21 October 2022

Please cite this article as: Pasquini L., Fryer S.L., Eisendrath S.J., Segal Z.V., Lee A.J., Brown J.A., Saggar M. & Mathalon D.H., Dysfunctional cortical gradient topography in treatment resistant major depression, *Biological Psychiatry: Cognitive Neuroscience and Neuroimaging* (2022), doi: https://doi.org/10.1016/j.bpsc.2022.10.009.

Title page

Title

Dysfunctional cortical gradient topography in treatment resistant major depression

Authors

Lorenzo Pasquini[1]*, Susanna L. Fryer[2, 3], Stuart J. Eisendrath[2], Zindel V. Segal[2], Alex J. Lee[1], Jesse A. Brown[1], Manish Saggar[4], Daniel H. Mathalon[2, 3]

Affiliations

[1]Department of Neurology, University of California, San Francisco

[2]Department of Psychiatry and Behavioral Sciences, University of California, San Francisco

[3]San Francisco Veteran Affairs Health Care System

[4]Department of Psychiatry and Behavioral Sciences Stanford University

***Corresponding author**

Lorenzo Pasquini, PhD. Email: Lorenzo.Pasquini@ucsf.edu

Running title

Brain gradients in treatment resistant major depression

Key words

Connectivity gradients, default mode network, functional connectivity, graph theory, treatment resistant major depression

Abstract

Background

Treatment-Resistant Depression (TRD) refers to patients with major depressive disorder who do not remit after two or more antidepressant trials. TRD is common and highly debilitating, but its neurobiological basis remains poorly understood. Recent neuroimaging studies have revealed cortical connectivity gradients that dissociate primary sensorimotor areas from higher-order associative cortices. This fundamental topography determines cortical information flow and is affected by psychiatric disorders. We examined how TRD impacts gradient-based hierarchical cortical organization.

Methods

In this secondary study, we analyzed resting-state fMRI data from a mindfulness-based intervention enrolling 56 TRD patients and 28 healthy controls. Using gradient extraction tools, baseline measures of cortical gradient dispersion within and between functional brain networks were derived, compared across groups, and associated with graph theoretical measures of network topology. In patients, correlation analyses were used to associate measures of cortical gradient dispersion with clinical measures of anxiety, depression, and mindfulness at baseline and following the intervention.

Results

Cortical gradient dispersion was reduced within major intrinsic brain networks in TRD. Reduced cortical gradient dispersion correlated with increased network degree assessed through graph theory-based measures of network topology. Lower dispersion among Default Mode, Control, and Limbic Network nodes related to baseline levels of trait anxiety, depression, and mindfulness.

Baseline Limbic Network dispersion in patients predicted trait anxiety scores 24 weeks after the intervention.

Conclusions

Our findings provide preliminary support for widespread alterations in cortical gradient architecture in TRD, implicating a significant role for transmodal and limbic networks in mediating depression, anxiety, and lower mindfulness in patients.

Introduction

Major depression is a common, debilitating disorder and among the leading causes of disability worldwide (1). Although several treatment options are available for depression, a significant number of patients do not improve despite adequate antidepressant trials (2). Patients that, after repeated treatments, do not reach acceptable levels of functioning and well-being, eventually present with treatment-resistant depression (TRD), a condition associated with a significant social and economic burden (2,3). TRD is often defined as the failure to remit after at least two antidepressant trials of adequate dose and duration (2,3). A consensus characterization of TRD, however, has yet to be achieved, partly due to a poor understanding of its neurobiological basis and a lack of reliable diagnostic biomarkers (4,5).

Resting-state fMRI (rs-fMRI) is a neuroimaging modality commonly used to measure functional connectivity of brain networks in terms of correlated spontaneous activity among distant brain regions (6,7). This method has proven useful in revealing altered functional connectivity within and between large-scale brain networks in depression (5,8–12). Crucially, brain network dysfunctions in major depression primarily affect limbic and higher-order associative systems including the Default Mode Network (DMN) (10,13,14), Control Network (CoN) (5,8–12), and

Limbic Network (LiN) (5,8–12), with imbalances in these systems being linked to emotional dysregulation and maladaptive self-referential processes, such as rumination (9,15,16).

Fundamental principles in behavioral neurology and recent neuroimaging studies provide convergent support for a hierarchical cortical organization that separates primary sensorimotor systems from transmodal associative areas (17–19). Cortical microstructure, connectivity, and gene expression findings point to dominant sensorimotor-to-transmodal gradients organizing the propagation of sensory inputs from primary areas into transmodal regions along multiple cortical relays (17,18,20). This large-scale brain system organization anchors the DMN at one end of the hierarchy with respect to primary sensorimotor areas, capturing a functional topography that enables the transition from perception to more abstract cognitive functions (9,15,16). Several neuropsychiatric disorders, including major depression (21), cognitive vulnerability to depression (22), and autism (20) profoundly impact connectivity-based cortical gradient organization. Major depression also disrupts global topography by producing focal alterations of cortical gradients among primary sensory and transmodal regions involved in high-order cognitive processing (21). Accordingly, we hypothesized that TRD would impact hierarchical brain network organization and that functional deficits affecting the DMN, CoN, and LiN would predict baseline and future symptoms of depression following group treatment with either mindfulness-based cognitive therapy (MBCT) or a health enhancement program (HEP). We retrospectively applied recently developed gradient decomposition techniques (23) to baseline rs-fMRI data from 56 TRD patients subsequently randomized to MBCT or HEP, and from 28 healthy controls (HC). This approach was leveraged to test the hypothesis that TRD, relative to HC, involves perturbation of hierarchical gradients among “canonical” large-scale brain networks (24). To aid with interpreting gradient-based deficits in network topography, we further contextualize the results by using a

complementary measure of nodal dysfunction based on network topology, specifically nodal degree (25).

Materials and Methods

Subjects

All participants or their surrogates provided written informed consent prior to participation in accordance with the declaration of Helsinki. The University of California, San Francisco (UCSF) Committee on Human Research approved the study.

An initial cohort of 59 TRD patients were enrolled in a randomized controlled behavioral intervention study that included baseline and post-treatment fMRI sessions, and 30 HC were recruited to provide normative baseline fMRI data. Participants were recruited from outpatient psychiatry and general medicine clinics at UCSF, the outpatient psychiatry clinic at Kaiser Permanente in San Francisco, and through advertisements and clinical referrals (26,27). TRD patient eligibility screening was completed in person. Eligible patients met Structured Clinical Interview for DSM-IV-TR Axis I (SCID-I/P) (28) criteria for major depression and had a Hamilton Depression Severity Rating Scale (HAMD-17) score of 14 or greater. Furthermore, to qualify as TRD, patients had to be taking antidepressant medication with evidence of two or more adequate trials prescribed during the current episode as assessed with the Antidepressant Treatment History Form (29). Patients were excluded for the following: lifetime history of bipolar disorder, schizophrenia, or any psychotic disorder; substance abuse or dependence within three months of study onset; currently suicidal, dangerous to others, or self-injurious; undergoing psychotherapy during the eight-week treatment portion of the study; or a score of <25 on the Mini Mental State Examination (30).

The HC group was matched to the TRD group on age, gender, and handedness and had no history of a major Axis I psychiatric disorder, neurological illness, or current use of psychotropic medication. Participants were required to be at least 18 years old, fluent in English, have no MRI contraindications, and to have normal or corrected-to-normal vision.

For each participant, we additionally assessed depressive symptoms through the Quick Inventory of Depression Symptomatology (QIDS-SR16) (31) and the Nolen-Hoeksema's Response Styles Questionnaire (RSQ22) (32); levels of mindfulness were assessed with the Five Facet Mindfulness Questionnaire (FFMQ) (33); and levels of state and trait anxiety were assessed through the State-Trait Anxiety Inventory (STAI trait and state) (34). Study participants self-reported race and ethnicity, sex, handedness, and years of education.

From the initially recruited sample, two HCs and three TRD patients had to be excluded based on excessive head movement in the scanner (see details below), resulting in the final analyzed sample of 56 TRD and 28 HC participants (Table 1).

Protocol

TRD patients were part of a randomized controlled trial comparing MBCT to a HEP as adjunctive treatments to ongoing antidepressant medication (26,27) Briefly, MBCT involved guided meditations (35); HEP involved activities to promote health (36). Patients were assessed with rs-fMRI at baseline and following intervention, while HC were assessed at baseline and did not undergo treatment (26,27). Of the 56 TRD included in our study, 27 went through the MBCT and 29 through the HEP intervention. Additional details are available in the Supplement and in previously published work. Only rs-fMRI data at baseline are analyzed in the present study.

Neuroimaging data acquisition and preprocessing

Neuroimaging data were acquired on a Siemens 3-T TIM TRIO scanner located at the UCSF Neuroimaging Center. A high-resolution anatomical scan was acquired using a 3-D MP-RAGE sequence, with scan time 5 min 17 s, flip angle 9 degrees, FOV = 220 mm, 160 slices per slab, 1.2 mm thick, no gap, TR = 2.30 s, TE = 2.94 ms. Functional scans were acquired using an EPI-BOLD sequence, TR = 2, TE= 30 ms, FoV = 220 MM, flip angle = 77 degrees, bandwidth = 2298 Hx/pixel, matrix = 64 x 64. 30 slices (3 mm thick, 1-mm gap). Scans were acquired in an axial-oblique plane, parallel to the anterior-posterior commissure (AC-PC) line. Participants were instructed to rest with eyes open during the 5 min and 24 s EPI-BOLD functional sequence.

The software fMRIPrep (https://fmriprep.org/en/stable/) (37) was used for data preprocessing. Anatomical MP-RAGE images were corrected for intensity non-uniformity, skull-stripped, and segmented for cerebrospinal fluid, white matter, and gray matter. Volume-based spatial normalization to MNI standard space was performed through nonlinear registration of the MP-RAGE with the T1-weighted MNI template brain (CBM152). The first five functional volumes were removed to allow for scanner equilibration, resulting in a total number of 157 volumes for the analyses. A mean reference volume and its skull-stripped version were generated, then co-registered to the structural reference using affine registration. Head-motion parameters (transformation matrices and the six corresponding rotation and translation parameters) were estimated and used to compute framewise head displacement time series. Functional images were slice-time corrected, realigned, and normalized to MNI standard space applying the structural transformation matrix to the co-registered functional data. The resulting volumes with 2 mm^3 isotropic resolution were spatially smoothed with a 6 mm radius Gaussian kernel and bandpass filtered in the 0.008–0.15 Hz frequency range. Nuisance parameters in the preprocessed data were

estimated for the cerebrospinal fluid and white matter. Additional nuisance parameters included the three translational and three rotational motion parameters, the temporal derivatives of the previous eight terms (white matter/cerebrospinal fluid/six motion time series), and the squares of the previous 16 terms (38,39). Nuisance parameters were filtered for the same frequency range as rs-fMRI data and regressed out from the filtered rs-fMRI data (38,39). The denoised data were used in subsequent analyses. Subjects were included only if their mean framewise head displacement in the scanner (38,39) was below the threshold of 0.55 mm recommended in previous work (40). Global signal regressed rs-fMRI data were also generated using the time series extracted from a whole-brain mask and used for control analyses.

Functional connectivity gradients

The Schaefer Atlas (41) was used to derive rs-fMRI activity time series for 400 cortical regions (Figure 1A-B). Pearson's correlation was applied to the regional activity time series to derive individual functional connectivity matrices (Figure 1Ca) and group-mean functional connectivity matrices for HC and TRD (Figure S1).

The diffusion embedding approach (17,18), as implemented by the toolbox BrainSpace (https://brainspace.readthedocs.io/en/latest/pages/getting_started.html) (23), was then applied to the HC group mean functional connectivity matrix to estimate connectivity gradients. Briefly, the top 10% strongest functional connections were retained for each parcel, referred to hereafter as a node, and cosine similarity was calculated between each pair of nodes to generate a dissimilarity matrix (Figure 1Cb) (42,43). Diffusion map embedding was then applied to decompose the functional connectome into primary components, referred to as gradients, with each gradient explaining varying levels of variance in connectivity (Figure 1Cc). These gradients discriminate across levels of the cortical hierarchy (i.e., sensory processing versus higher-order cognition),

whereas node-specific gradient values reflect the similarity in connectivity along this sensory-transmodal axis. An identical approach was used to derive connectivity gradients from the TRD group mean connectivity matrix and from the connectivity matrices of individual participants. The resulting gradient maps were subsequently aligned to the gradients derived at the group-level in HCs using iterative Procrustes rotation, therefore enabling comparisons across individual embedding solutions (20,23,44). Control analyses were performed with publicly available cortical gradients maps (17) (see Supplement).

Nodal dispersion

For each participant, we then derived a measure of within-network nodal dispersion. We plotted the first three connectivity gradients – since these explained most of the underlying variance (see elbow plot in Figure 1 Cc) – against each other to derive a three-dimensional manifold in which we calculated the Euclidean distance between nodes belonging to the same intrinsic brain network (44) (Figure 1Cd). Nodal dispersion was derived for each node belonging to a specific intrinsic brain network and averaged across nodes within intrinsic brain networks, yielding a final estimate of within-network nodal dispersion for each participant. We performed several control analyses to assess the impact of methodological parameters on our analyses (see Supplement). Further, we derived a measure of between-network nodal dispersion calculated as the Euclidean distance between network centroids (i.e., the arithmetic mean in gradient space of all nodes belonging to the same network).

Nodal degree

In parallel to the connectivity gradient approach, we also derived a traditional measure of within-network nodal degree for all participants (25) by using the publicly available Brain Connectivity Toolbox (https://sites.google.com/site/bctnet/).

Nodal degree is a widely used measure of network topology commonly derived using graph-theoretical approaches (25). Briefly, individual connectivity matrices were thresholded for correlation values below 0.35 (retaining a median of 26% of connections) and binarized (Figure 1Ce). To control for threshold choice, measures of nodal degree were derived also for connectivity thresholds of 0.45 and 0.25 (respectively retaining 16% and 38% of connections). At any threshold, patients and controls did not significantly differ in respect to the density of retained connections. Weighted connectivity matrices were used to count the number of surviving edges between a specific node within a network and all other nodes within the same network (Figure 1Cf). The sum of surviving edges for a node was then divided by the total amount of edges within the network. Nodal degree measures were derived for each single node in a network and averaged across nodes in the same network. This procedure resulted in a measure of within-network nodal degree reflecting the level of integration between nodes belonging to the same network.

Statistical analyses

In house MATLAB R2021a (https://www.mathworks.com/products/matlab.html) and R 4.1.1 (https://www.r-project.org/) scripts were used to perform the statistical analyses. See Supplementary Methods for more details.

Results

Cortical connectivity gradients in HCs and TRD

We applied a diffusion gradient approach separately on rs-fMRI-based connectivity data from HCs and TRD to derive cortical connectivity gradients reflecting processing hierarchies spanning sensory and transmodal areas (Figure 2 and Figure S2A). The first three principal gradients derived from rs-fMRI data of HCs, explained 34.9% of the variance in functional connectivity (elbow plot in Figure 1 Cc). Gradient 1 anchored sensorimotor areas at its positive extreme, while

regions belonging to the DMN were located at the opposite, negative extreme (Figure 2A-B). Sensorimotor and DMN areas occupied the negative extreme on Gradient 2, while visual-sensory areas populated the positive end of this gradient (Figure 2A-B). Notably, these first two connectivity gradients overlap with previously reported gradients in functional connectivity, structural connectivity, myelin density, and genetic expression (17,18), which consistently separate sensory processing regions from transmodal areas of the DMN. Gradient 3 showed a more complex pattern, segregating regions of the Dorsal Attention Network from regions belonging to the Salience Network, potentially reflecting a higher-order, attention-related gradient separating regions attending to externally presented cues (45) from regions devoted to processing visceral and interoceptive information (46,47). The normative gradients identified in our HCs sample showed strong to moderate correspondence to gradients described in prior foundational work (Figure 2C) (17). Similar fundamental properties of hierarchical brain organization were found in patients with TRD after aligning the principal connectivity gradients of patients to those of HCs (Figure 2D-E), in support of the notion that cortical gradients reflect fundamental properties of brain topography in both health and disease (17,18,20,21). Gradients 4-6 explained a lower amount of variance and showed less discernible patterns of regional variation (Figure S2).

Within-network nodal dispersion

Node-level gradient comparisons ($p<0.05$, uncorrected) revealed increased gradient scores in TRD patients in sensory and early transmodal regions, such as the ventromedial occipital and posterior inferior temporal cortices, together with decreased gradient scores in transmodal areas including the precuneus, the medial prefrontal, and cingulate cortices (Figure 3A). We then derived a measure of within-network nodal dispersion (Figure 1Cd), reflecting the level of connectedness of nodes belonging to the same intrinsic brain network (44). A two-way analysis of variance revealed

a main effect of network, $F(6,567)=15.2$, $p<0.0005$, and an main effect of group, $F(2,567)=18.0$, $p<0.0005$. Pair-wise comparisons revealed that all networks, except for the Salience and Sensorimotor Networks, showed reduced within-network nodal dispersion in TRD compared to HCs (Figure 3B; $p<0.05$, FDR corrected for multiple comparisons), suggesting overall higher within-network connectedness. We performed control analyses to assess the impact of head movement on within-network dispersion and assessed the impact of methodological parameters including (i) global signal regression; (ii) atlas parcellation; (iii) gradient decomposition through Laplacian embedding; (iv) angular normalization to generate the dissimilarity matrices; (v) adding Gradients 4-6 when computing within-network nodal dispersion; or (vi) using publicly available gradient maps to derive individual gradients (see Supplementary Results, Figures S2-S4, and Tables S1-S2).

We analyzed whether TRD also affected cortical hierarchies between networks in addition to within-network gradient organization. We derived a measure of between-network nodal dispersion that revealed reduced nodal dispersion in TRD between the Sensorimotor and the DMN, between the Salience and the DMN, and between the CoN and Dorsal Attention Network, although none of these findings survived correction for multiple comparisons (Figure 4; $p<0.05$, uncorrected).

Within-network nodal degree

Comprehensively, the previous findings suggested that in TRD, nodes belonging to the same network are more integrated to each other. To confirm this hypothesis, we derived a complementary measure of nodal integration based on graph theoretical approaches, namely within-network nodal degree. A two-way analysis of variance revealed a main effect of network, $F(6,567)=187.9$, $p<0.0005$, and a weaker main effect of group, $F(2,567)=3.1$, $p<0.05$. Pair-wise comparisons revealed that there were no significant between-group differences in within-network

degree that survived multiple comparisons. However, DMN and Sensorimotor Network nodal degree was significantly lower in TRD compared to HCs (Figure 3C; $p<0.05$, uncorrected).

When relating within-network nodal dispersion to within-network nodal degree, we consistently found a significant negative association between both measures, particularly in TRD and to a lesser extent in HCs (Figure 3D; $p<0.05$, FDR corrected for multiple comparisons if not reported otherwise, Pearson's correlation coefficients and associated Fisher r-to-z tests for independent samples comparing the strength of correlations across groups reported in the plots). Notably, these findings were robust across distinct thresholds applied to generate the weighted connectivity matrices used to estimate nodal degree (Figure S3). In summary, these findings support the notion that decreased within-nodal dispersion, at least in patients, reflects within-network hyper-connectedness. This negative association between nodal measures was prominent in TRD but not as prominent in HCs, suggesting a more complex relationship between cortical topology and topography in the healthy human brain.

Within-network nodal dispersion and baseline symptoms of depression

Given the recurrent association of the DMN, CoN and LiN with clinical symptoms of depression (9,15,16), we first investigated the association of within-network nodal dispersion and degree in these systems with clinical depression severity in patients as assessed with the HDRS-17. Within-network nodal dispersion of any network did not significantly correlate with HDRS-17, although within-network nodal degree of the CoN and LiN positively correlated with HDRS scores (Table S3). Subsequently, we assessed the relationship between within-network nodal dispersion of the DMN, CoN, and LiN and clinical measures of increased anxiety, depressed mood, and reduced mindfulness (16,26,27). To assess whether associations between nodal dispersion and clinical measures were specific to higher-order cognitive and emotional systems, we also report

correlations between clinical measures and nodal dispersion of the Visual Network. In line with previous work, our patient sample showed increased levels of trait anxiety as measured through the STAI questionnaire (Figure 5A; $p<0.0005$), increased levels of depressive symptoms using the RSQ22 (Figure 5B; $p<0.0005$), and decreased levels of mindfulness (26,27) as measured through the FFMQ (Figure 5C; $p<0.0005$). Within-network nodal dispersion of the DMN, CoN and LiN negatively correlated with trait anxiety and depression while it positively correlated with mindfulness in patients but not in HCs (Figure 5D-E). Dispersion of the Visual Network did not significantly correlate with any clinical measure. Consistent with the previously described negative relationship between nodal dispersion and nodal degree, within-network nodal degree of the DMN, CoN, and LiN positively correlated with trait anxiety and depression while it negatively correlated with mindfulness in patients but not in HCs (Figure 5G-I).

Within-network nodal dispersion and change scores in clinial symptoms

In line with our previous studies (26,27), patients on the MBCT arm showed greater HDRS-17 reductions relative to the control intervention, although in our study the effect only reached trending significance ($F(1,107)=3.07$; $p=0.08$; Figure S5) (26,27), likely due to the smaller patient subset in this sample following head-movement control. We then assessed whether within-network nodal dispersion at baseline could predict STAI trait, FFMQ, and RSQ22 change scores, since these clinical questionnaires correlated with baseline nodal dispersion. A repeated measurement ANOVA revealed a main effect of time (but no effect of group), with improved STAI trait, FFMQ, and RSQ22 scores after 8 and 24 weeks in both the HEP and MBCT arms (Figure S6 and Table S4). Multiple regression analyses revealed that LiN nodal dispersion at baseline predicted STAI trait change scores 24 weeks after the intervention (Figure 6; $\beta(1,46)=0.63$; $p=0.01$).

Discussion

Functional connectivity of the human cortex can be decomposed in primary gradients that anchor, on one end, primary sensory and motor areas and on the other end, transmodal regions overlapping with the DMN. This study explored how TRD impacts this fundamental topography of hierarchical cortical organization. We capitalized on rs-fMRI data acquired in TRD patients and HCs and applied recently developed gradient extraction tools to assess gradient imbalances within major intrinsic brain networks. Although the global hierarchical architecture was similar across the two groups, we found that brain regions belonging to the same network are located more closely to each other in topographical gradient space in TRD relative to HCs. Reduced within-network nodal dispersion correlated with higher levels of nodal degree derived through graph theory-based topology measures, overall suggesting higher within-network functional integration in TRD. In patients, decreased nodal dispersion of higher-order cognitive and limbic networks correlated with depression, anxiety, and reduced mindfulness at baseline. Change in anxiety scores following a mindfulness-based intervention were predicted by limbic nodal dispersion. Overall, these findings suggest deleterious cortical network topography and topology in TRD and underscore the role of higher-order and limbic networks in mediating core symptoms of depression.

Increased within-network integration in TRD

The pervasive correlation between nodal degree and nodal dispersion in our patient sample suggests that TRD impacts cortical hierarchies by driving hyper-integration within several brain networks (48). Other neuropsychiatric conditions have been shown to impact cortical connectivity gradients. Autism spectrum disorder has been shown to alter brain topography by showing atypical connectivity transitions between sensory and higher-order DMN regions (20). Our findings align with previous reports of altered cortical gradient organization in individuals with cognitive

vulnerability to depression (22) and in a larger sample of patients with major depression (21). Individuals with cognitive vulnerability to depression have been shown to display reduced gradient scores in the left insula, which correlated with lower attentional scores in patients, suggesting that gradient reorganization may precede the onset of depression (22). A recent study involving a large sample of patients showed that major depressive disorder exhibits abnormal global topography of the principal sensory-to-transmodal gradient (21). These focal alterations of gradient scores mostly affected transmodal areas implicated in higher-order cognition overlapping with the DMN (21).

Brain network hyper-integration mediates symptoms of depression

Despite numerous efforts to map brain network dysfunctions in depression, important inconsistencies exist regarding the location and directionality of connectivity changes, with both hyper- (15), and hypo-connectivity findings reported in the literature (49). Disease duration, perseverance of symptoms, and heterogenous subtypes of depression (8,9) may account for important sources of variability, as do head movement in the scanner, and differing data acquisition protocols and preprocessing pipelines (38–40). Although our findings contrast with reports of decreased connectivity in attentional networks (10), they align well with previous reports of DMN hyper-connectivity found in patients with depression (9,15). Hyper-connectivity among DMN regions in depression is consistent with our interpretation of reduced nodal dispersion reflecting within-network hyper-integration. Prior studies in both HCs and depression have associated DMN hyper-synchrony with self-referential processes affected in depression, including reduced mindfulness and social-emotional dysfunctions (15,16,50), suggesting a deleterious nature of DMN hyper-integration in TRD.

Limitations and future directions

Three limitations need to be considered when interpreting our findings as potential evidence of within-network hyper-integration in TRD. First, methods used to extract connectivity gradients may need further refinements when addressing gradient changes at the individual level and across clinical populations. Although findings of reduced within-network nodal dispersion were consistently found when using global signal regression or medium to high parcellated atlases, the method chosen to derive cortical connectivity gradients greatly influenced the analyses. Second, nodal dispersion in TRD did not correlate with HDRS-17 nor, except for the LiN, predicted clinical improvement following either MBCT or HEP. Gradient approaches have been mostly applied to study fundamental aspects of brain functioning by leveraging large samples. Our analyses may have suffered from sample size issues affecting both patients and controls. Given the recent discovery of distinct biotypes in major depressive disorder (8,9), longitudinal studies involving larger patient samples are needed to validate our findings. Future studies should confirm whether decreased nodal dispersion is a generalizable marker of network hyper-integration in TRD, and whether nodal dispersion can be normalized following tailored behavioral and pharmacological interventions.

Acknowledgements

This work was supported by NIH grant K99-AG065457 to LP, DP2-MH119735 to MS, NIH/NCCAM grant R01-AT004572-02S1 to SJE and DHM. We thank the participants and their families for their contributions to depression research.

Disclosures

The authors report no biomedical financial interests or potential conflicts of interest. Participants' data is not publicly shared due to privacy concerns but is available from the senior author after reasonable request. Code is available on https://github.com/lollopasquini.

References

1. Evans-Lacko S, Aguilar-Gaxiola S, Al-Hamzawi A, Alonso J, Benjet C, Bruffaerts R, *et al.* (2018): Socio-economic variations in the mental health treatment gap for people with anxiety, mood, and substance use disorders: Results from the WHO World Mental Health (WMH) surveys. *Psychological Medicine* 48.

2. Berlim MT, Turecki G (2007): Definition, assessment, and staging of treatment-resistant refractory major depression: A review of current concepts and methods. *Canadian Journal of Psychiatry*, vol. 52.

3. Fava M, Davidson KG (1996): Definition and epidemiology of treatment-resistant depression. *Psychiatric Clinics of North America* 19.

4. Klok MPC, van Eijndhoven PF, Argyelan M, Schene AH, Tendolkar I (2019): Structural brain characteristics in treatment-resistant depression: review of magnetic resonance imaging studies. *BJPsych Open* 5.

5. de Kwaasteniet BP, Rive MM, Ruhé HG, Schene AH, Veltman DJ, Fellinger L, *et al.* (2015): Decreased Resting-State Connectivity between Neurocognitive Networks in Treatment Resistant Depression . *Frontiers in Psychiatry* , vol. 6. p 28.

6. Fox MD, Snyder AZ, Vincent JL, Corbetta M, Essen DC van, Raichle ME (2005): The human brain is intrinsically organized into dynamic , anticorrelated functional networks. *Proc Natl Acad Sci U S A* 102: 9673–9678.

7. Smith SM, Fox PT, Miller KL, Glahn DC, Fox PM, Mackay CE, *et al.* (2009): Correspondence of the brain's functional architecture during activation and rest. *Proc Natl Acad Sci U S A* 106: 13040–5.

8. Drysdale AT, Grosenick L, Downar J, Dunlop K, Mansouri F, Meng Y, *et al.* (2017): Resting-state connectivity biomarkers define neurophysiological subtypes of depression. *Nature Medicine* 23: 28–38.

9. Williams LM (2016): Precision psychiatry: A neural circuit taxonomy for depression and anxiety. *The Lancet Psychiatry* 3: 472–480.

10. Kaiser RH, Pizzagalli DA (2015): Large-Scale Network Dysfunction in Major Depressive Disorder- A Meta-analysis of Resting-State Functional Connectivity. *JAMA Psychiatry*.

11. Zheng H, Xu L, Xie F, Guo X, Zhang J, Yao L, Wu X (2015): The altered triple networks interaction in depression under resting state based on graph theory. *BioMed Research International* 2015: 9–12.

12. Kaiser RH, Whitfield-Gabrieli S, Dillon DG, Goer F, Beltzer M, Minkel J, *et al.* (2016): Dynamic Resting-State Functional Connectivity in Major Depression. *Neuropsychopharmacology* 41: 1822–1830.

13. Buckner RL, DiNicola LM (2019): The brain's default network: updated anatomy, physiology and evolving insights. *Nat Rev Neurosci*.

14. Raichle ME, MacLeod AM, Snyder AZ, Powers WJ, Gusnard DA, Shulman GL (2001): A default mode of brain function. *Proceedings of the National Academy of Sciences* 98: 676 LP – 682.

15. Sheline YI, Price JL, Yan Z, Mintun MA (2010): Resting-state functional MRI in depression unmasks increased connectivity between networks via the dorsal nexus. *Proceedings of the National Academy of Sciences* 107: 11020 LP – 11025.

16. Sheline YI, Barch DM, Price JL, Rundle MM, Vaishnavi SN, Snyder AZ, *et al.* (2009): The default mode network and self-referential processes in depression. *Proceedings of the National Academy of Sciences* 106: 1942 LP – 1947.

17. Margulies DS, Ghosh SS, Goulas A, Falkiewicz M, Huntenburg JM, Langs G, *et al.* (2016): Situating the default-mode network along a principal gradient of macroscale cortical organization. *Proceedings of the National Academy of Sciences* 113: 12574–12579.

18. Huntenburg JM, Bazin PL, Margulies DS (2018): Large-Scale Gradients in Human Cortical Organization. *Trends in Cognitive Sciences* 22: 21–31.

19. Mesulam MM (1990): Large-scale neurocognitive networks and distributed processing for attention, language, and memory. *Annals of Neurology* 28: 597–613.

20. Hong S-J, Vos de Wael R, Bethlehem RAI, Lariviere S, Paquola C, Valk SL, *et al.* (2019): Atypical functional connectome hierarchy in autism. *Nature Communications* 10: 1022.

21. Xia M (2022): Connectome gradient dysfunction in major depression and its association with gene expression profiles and treatment outcomes. *Mol Psychiatry* 27(3):1384-1393.

22. Wang J, Zhou Y, Ding J, Xiao J (2021): Functional gradient alteration in individuals with cognitive vulnerability to depression. *Journal of Psychiatric Research*.

23. Vos de Wael R, Benkarim O, Paquola C, Lariviere S, Royer J, Tavakol S, *et al.* (2020): BrainSpace: a toolbox for the analysis of macroscale gradients in neuroimaging and connectomics datasets. *Communications Biology* 3.

24. Yeo BTT, Krienen FM, Sepulcre J, Sabuncu MR, Lashkari D, Hollinshead M, *et al.* (2011): The organization of the human cerebral cortex estimated by intrinsic functional connectivity. *J Neurophysiol* 106: 1125–1165.

25. Rubinov M, Sporns O (2010): Complex network measures of brain connectivity: Uses and interpretations. *Neuroimage* 52: 1059–1069.

26. Eisendrath SJ, Gillung E, Delucchi KL, Zindel V, Nelson JC, Mcinnes LA, *et al.* (2016): A Randomized Controlled Trial of Mindfulness-Based Cognitive Therapy for Treatment-Resistant Depression Stuart. *Psychother Psychosom* 85: 99–110.

27. Ferri J, Eisendrath SJ, Fryer SL, Gillung E, Roach BJ, Mathalon DH (2017): Blunted amygdala activity is associated with depression severity in treatment-resistant depression. *Cognitive, Affective and Behavioral Neuroscience* 17: 1221–1231.

28. First MB, Pincus HA (2002): The DSM-IV Text Revision: Rationale and potential impact on clinical practice. *Psychiatric Services* 53.

29. Sackeim HA (2001): The definition and meaning of treatment-resistant depression. *Journal of Clinical Psychiatry*, vol. 62.

30. Folstein MF, Folstein SE MP (1975): Mini-mental state. A grading the cognitive state of patiens for the clinician. *J Psychiatr Res* 12: 189–198.

31. Rush AJ, Trivedi MH, Ibrahim HM, Carmody TJ, Arnow B, Klein DN, *et al.* (2003): The 16-item Quick Inventory of Depressive Symptomatology (QIDS), clinician rating (QIDS-C), and self-report (QIDS-SR): A psychometric evaluation in patients with chronic major depression. *Biological Psychiatry* 54.

32. Nolen-Hoeksema S, Morrow J (1991): A Prospective Study of Depression and Posttraumatic Stress Symptoms After a Natural Disaster: The 1989 Loma Prieta Earthquake. *Journal of Personality and Social Psychology* 61.

33. Baer RA, Smith GT, Hopkins J, Krietemeyer J, Toney L (2006): Using self-report assessment methods to explore facets of mindfulness. *Assessment* 13.

34. Spielberger C, Gorsuch R, Lushene R (1970): STAI manual for the state-trait anxiety inventory. Self-Evaluation Questionnaire. *Lushene Consulting Psychologists Press*.

35. Segal Z v, Williams JMG, Teasdale JD (2013): Mindfulness-based cognitive therapy for depression, 2nd ed. *Mindfulness-Based Cognitive Therapy for Depression, 2nd Ed.* New York, NY, US: The Guilford Press.

36. MacCoon DG, Imel ZE, Rosenkranz MA, Sheftel JG, Weng HY, Sullivan JC, *et al.* (2012): The validation of an active control intervention for Mindfulness Based Stress Reduction (MBSR). *Behaviour Research and Therapy* 50.

37. Esteban O, Markiewicz CJ, Blair RW, Moodie CA, Ayse I, Erramuzpe A, *et al.* (2018): FMRIPrep : a robust preprocessing pipeline for functional MRI. 5: 1–20.

38. Power JD, Mitra A, Laumann TO, Snyder AZ, Schlaggar BL, Petersen SE (2014): NeuroImage Methods to detect, characterize, and remove motion artifact in resting state fMRI. *Neuroimage* 84: 320–341.

39. Satterthwaite TD, Elliott MA, Gerraty RT, Ruparel K, Loughead J, Calkins ME, *et al.* (2013): An improved framework for confound regression and filtering for control of motion artifact in the preprocessing of resting-state functional connectivity data. *Neuroimage* 64: 240–256.

40. Parkes L, Fulcher B, Yücel M, Fornito A (2018): An evaluation of the efficacy, reliability, and sensitivity of motion correction strategies for resting-state functional MRI. *Neuroimage* 171: 415–436.

41. Schaefer A, Kong R, Gordon EM, Laumann TO, Zuo X-N, Holmes AJ, *et al.* (2018): Local-Global Parcellation of the Human Cerebral Cortex from Intrinsic Functional Connectivity MRI. *Cerebral Cortex* 28: 3095–3114.

42. Larivière S, Vos de Wael R, Hong S-J, Paquola C, Tavakol S, Lowe AJ, *et al.* (2020): Multiscale Structure–Function Gradients in the Neonatal Connectome. *Cerebral Cortex* 30: 47–58.

43. Paquola C, Vos De Wael R, Wagstyl K, Bethlehem RAI, Hong S-J, Seidlitz J, *et al.* (2019): Microstructural and functional gradients are increasingly dissociated in transmodal cortices. *PLOS Biology* 17: e3000284.

44. Bethlehem RAI, Paquola C, Seidlitz J, Ronan L, Bernhardt B, Consortium CCAN, Tsvetanov KA (2020): Dispersion of functional gradients across the adult lifespan. *Neuroimage* 222.

45. Corbetta M, Shulman GL (2002): Control of Goal-Directed and Stimulus-Driven Attention in the Brain. *Nature Reviews Neuroscience* 3: 215–229.

46. Seeley WW (2019): The salience network : a neural system for perceiving and responding to homeostatic demands. *Journal of Neuroscience*.

47. Critchley HD, Harrison NA (2013): Visceral Influences on Brain and Behavior. *Neuron* 77: 624–638.

48. Daws RE, Timmermann C, Giribaldi B, Sexton JD, Wall MB, Erritzoe D, *et al.* (2022): Increased global integration in the brain after psilocybin therapy for depression. *Nature Medicine*.

49. Yan CG, Chen X, Li L, Castellanos FX, Bai TJ, Bo QJ, *et al.* (2019): Reduced default mode network functional connectivity in patients with recurrent major depressive disorder. *Proc Natl Acad Sci USA* 116: 9078–9083.

50. Farb NAS, Desormeau P, Anderson AK, Segal Z v. (2022): Static and treatment-responsive brain biomarkers of depression relapse vulnerability following prophylactic psychotherapy: Evidence from a randomized control trial. *NeuroImage: Clinical* 34: 102969.

Tables and Legends

Figure 1. Analytic pipeline. (A) 400 nodes from the Schaefer Atlas, each overlapping with a specific intrinsic brain network (IBN) **(B)**, were used to derive functional connectivity matrices using rs-fMRI data of HCs and patients with TRD. **(Ca).** Individual connectivity matrices (Si) went through two distinct processing pipelines. To derive cortical connectivity gradients (upper stream), individual connectivity matrices were transformed to affinity matrices using cosine similarity (**Cb**) and Laplacian decomposition was used to derive three primary connectivity gradients, which combined explained 34.9% of the variance in functional connectivity (**Cc**). The position of an individual node belonging to a specific intrinsic brain network (e.g. Network x) was used to derive a topographical measure of nodal dispersion (**Cd**), reflecting the average Euclidean distance in gradient space between a node and all other nodes belonging to the same network. Individual connectivity matrices were also leveraged to derive topological measures of nodal degree (lower stream). Connectivity matrices were weighted by binarizing at a connectivity threshold of 0.35 (**Ce**). For each node within a network, we assessed the level of degree by counting the edges of this node to all other nodes within a network and dividing by the total amount of edges (**Cf**). CoN = Control Network; DAN = Dorsal Attention Network; DMN = Default Mode Network; HC = healthy controls; LiN = Limbic Network; SaN = Salience Network; SMN = Sensorimotor network; TRD = patients with treatment resistant depression; ViN = Visual Network.

Figure 2. Cortical connectivity gradients. (A) Cortical connectivity gradients of HCs projected into cortical surface. The three-dimensional scatterplot below shows how individual nodes distribute along the first three gradients. Colors reflect the loadings of nodes on individual gradients. For example, the sensorimotor cortex appears purple and regions overlapping with the DMN appear blue, reflecting that these systems respectively anchor the extremes of Gradient 1. **(B)** Scatterplots reflecting how nodes belonging to distinct intrinsic brain networks align along cortical gradients in HC. **(C)** Spatial correlation between maps of Gradients 1-3 in HCs and maps of Gradients 1-3 using publicly available maps of canonical cortical gradients. **(D)** Cortical connectivity gradients of patients with TRD aligned to the gradients of HCs following Procrustes rotation. **(E)** Scatterplots reflecting how nodes belonging to distinct intrinsic brain networks align along cortical gradients in patients with TRD. CoN = Control Network; DAN = Dorsal Attention Network; DMN = Default Mode Network; HC = healthy controls; LiN = Limbic Network; SaN = Salience Network; SMN = Sensorimotor network; TRD = patients with treatment resistant depression; ViN = Visual Network. *$p<0.005$

554 **Figure 3. Nodal dispersion and nodal degree. (A)** Node-wise statistical comparisons between
555 HCs and TRD, with increases/decreases in TRD shown in cold/warm colors ($p<0.05$ uncorrected).
556 **(B)** Violinplots reflecting topographical differences in within-network nodal dispersion between
557 patients with TRD (red) and HCs (blue). **(C)** Violinplots reflecting topological differences in
558 within-network nodal degree between patients with TRD and HCs. **(D)** Scatterplots reflecting the
559 association between within-network nodal degree and within-network nodal dispersion separately
560 for patients with TRD and HCs. Pearson's correlation coefficients are reported below the
561 scatterplots for each group separately, together with associated Fisher r-to-z tests for independent
562 samples comparing the strength of the correlations across groups. CoN = Control Network; DAN
563 = Dorsal Attention Network; DMN = Default Mode Network; HC = healthy controls; LiN =
564 Limbic Network; SaN = Salience Network; SMN = Sensorimotor network; TRD = patients with
565 treatment resistant depression; ViN = Visual Network. *$p<0.05$ FDR corrected, +$p<0.05$
566 uncorrected
567

Figure 4. Between-network nodal dispersion. Between-network nodal distance in **(A)** HCs and **(B)** patients with TRD. **(C)** Significant reductions in between-network nodal dispersion were found in patients with TRD, affecting the Sensorimotor and DMN, the Salience and DMN, and the Control and Dorsal Attention Network. None of these findings survived FDR correction for multiple comparisons. *$p<0.05$ uncorrected. CoN = Control Network; DAN = Dorsal Attention Network; DMN = Default Mode Network; HC = healthy controls; LiN = Limbic Network; SaN = Salience Network; SMN = Sensorimotor network; TRD = patients with treatment resistant depression; ViN = Visual Network.

Figure 5. Nodal dispersion correlates with symptoms of depression. (A) Levels of trait anxiety (STAI trait total scores) and **(B)** depression (RSQ22) are significantly higher in patients with TRD (red violinplots) when compared to HCs (blue violinplots), while levels of **(C)** mindfulness (FFMQ total scores) are significantly lower in patients when compared to HCs. **(D)** Within-network nodal dispersion of the DMN, CoN, and LiN correlate negatively with trait anxiety and depression and positively with mindfulness in TRD patients but not in HCs **(E)**. No significant correlations were found for dispersion of the ViN, suggesting a specific association of clinical measures to higher-order cognitive and limbic networks. Matrix in **(F)** reflects Fisher r-to-z tests for independent samples comparing the strength of the correlations across groups. **(G)** Conversely, within-network nodal degree of the DMN, CoN, and LiN correlate positively with trait anxiety and depression and negatively with mindfulness in TRD patients but not in HCs **(H)**. Matrix in **(I)** reflects Fisher r-to-z tests for independent samples comparing the strength of the correlations across groups. CoN = Control Network; DMN = Default Mode Network; HC = healthy controls; LiN = Limbic Network; TRD = patients with treatment resistant depression. ***$p<0.0005$, **$p<0.005$, *$p<0.05$, $^{+}p<0.1$

Figure 6. Baseline LiN nodal dispersion predicts change in STAI trait following a MBCT/HEP intervention. (A) Parameter regression coefficients from multiple regression models predicting clinical score changes (Baseline – 24 weeks) from baseline within-network nodal dispersion. **(B)** Only nodal dispersion of the LiN significantly predicted STAI strait change scores. CoN = Control Network; DMN = Default Mode Network; HEP = health enhancement program; LiN = Limbic Network; MBCT = mindfulness-based cognitive therapy. *$p<0.05$; +$p<0.01$

599

	HC (n=28)	TRD (n=56)	T	p
Age in years	45.4 (9.3)	42.9 (9.9)	1.14	0.260
Female	20	44	0.21[&]	0.651
Handedness ambidextrous/left/right	1/2/25	2/5/49	0.08[&]	0.962
Education in years	16.9 (2.5)	16.1 (2.1)	1.57	0.123
Hispanic-Latino	4	4	0.40[&]	0.529
Asian/Black/Other/White	1/2/0/25	6/4/1/45	12.38[&]	<0.01
Mean FD in mm	0.23 (0.10)	0.25 (0.11)	-1.01	0.316
Mean spike occurrence: number of volumes with FD>0.5mm	7.5 (14.4)	13.4 (18.9)	1.45	0.149
Age of MDE onset in years	-	20.8 (10.1)	-	-
Number of MDEs	-	3.6 (2.5)	-	-
Current onset duration in months	-	85.6 (110.5)	-	-
Number of trials	-	2.9 (1.3)	-	-
Concurrent medication at baseline				
Antidepressants	-	56 (100.0%)	-	-
Mood stabilizers	-	8 (14.3%)	-	-
Sedatives	-	19 (33.9%)		
Stimulants	-	13 (23.2%)	-	-
Antipsychotics	-	1 (20.0%)	-	-
Other	-	1 (1.8%)	-	-

Clinical questionnaires				
HDRS-17	1.6 (1.3)	17.4 (2.7)	-35.5	<0.001
QIDS-SR16	2.6 (1.4)	14.9 (3.7)	-21.6	<0.001
STAI trait	27.6 (5.8)	60.1 (8.5)	-19.6	<0.001
STAI state	26.5 (7.8)	56.3 (9.8)	-14.5	<0.001
RSQ22	31.8 (9.0)	59.7 (11.0)	-12.0	<0.001
FFMQ	157.2	106.1	12.0	<0.001

Table 1. Participants' demographic and clinical characteristics at baseline. Mean and standard deviation in brackets. [&]Chi-square test. FD = framewise head displacement; FFMQ = Five Facet Mindfulness Questionnaire; HDRS-17 = Hamilton Depression Rating Scale; HC = healthy control; MAOI = monoamine oxidase inhibitors; MDE = major depressive episode; QIDS-SR16 = Quick Inventory of Depression Symptomatology; RSQ22 = Nolen-Hoeksema's Response Styles Questionnaire; SNRI = selective and norepinephrine reuptake inhibitors; SRI = selective reuptake inhibitors; SSRI = selective serotonin reuptake inhibitors; STAI = State-Trait Anxiety Inventory; TCA = tricyclic antidepressants; TRD = treatment resistant major depression.